PCCP

Hyper-Rayleigh Scattering in 2D Redox Exfoliated Semi-metallic $ZrTe_2$ Transition Metal Dichalcogenide

Journal:	*Physical Chemistry Chemical Physics*
Manuscript ID	CP-ART-09-2020-004821.R2
Article Type:	Paper
Date Submitted by the Author:	20-Nov-2020

Complete List of Authors:	Silva Neto, Manoel; Universidade Federal de Pernambuco Centro de Ciencias Exatas e da Natureza, Programa de Pós-Graduação em Ciência de Materiais, Universidade Federal de Pernambuco, Recife, PE 50740-560, Brazil Silva, Renato; Universidade Federal de Pernambuco, Departamento de Física de Araújo, Cid Bartolomeu; Universidade Federal de Pernambuco, Departamento de Física; Universidade Federal de Pernambuco Centro de Ciencias Exatas e da Natureza, Programa de Pós-Graduação em Ciência de Materiais, Universidade Federal de Pernambuco, Recife, PE 50740-560, Brazil de Matos, Christiano; Mackenzie Presbyterian University, MackGraphe Jawaid, Ali; Air Force Research Laboratory, Materials and Manufacturing Directorate Ritter, Allyson; Air Force Research Laboratory, Materials and Manufacturing Directorate Vaia, Richard; Air Force Research Laboratory, Materials and Manufacturing Gomes, Anderson; Universidade Federal de Pernambuco, Departamento de Física

ARTICLE

Hyper-Rayleigh Scattering in 2D Redox Exfoliated Semi-metallic $ZrTe_2$ Transition Metal Dichalcogenide

Manoel L. da Silva-Neto[a], Renato Barbosa-Silva[b], Cid B. de Araújo[a,b], Christiano J. S. de Matos[c], Ali M. Jawaid[d], Allyson J. Ritter[d], Richard A Vaia[d] and Anderson S. L. Gomes[b]

Received 00th January 20xx,
Accepted 00th January 20xx

DOI: 10.1039/x0xx00000x

Nonlinear optical characterization of nanostructured layered transition metal dichalcogenides (LTMDs) is of fundamental interest for basic knowledge and applied purposes. In particular, second-order optical nonlinearities are the basis for second harmonic generation as well as sum or difference frequency generation and have been studied in some 2D TMDs, especially in those with a semiconducting character. Here we report, for the first time, on the second-order nonlinearity of the semi-metallic $ZrTe_2$ monolayer in acetonitrile suspension (concentration of 4.9×10^{10} particles$/cm^3$), synthesized via a modified redox exfoliation method and characterized using the hyper-Rayleigh scattering technique in the nanosecond regime. The orientation-averaged first-hyperpolarizability was found to be $\beta(2\omega) = (7.0 \pm 0.3) \times 10^{-24}$esu per $ZrTe_2$ monolayer flake, the largest reported so far. Polarization-resolved measurements were performed in the monolayer suspension and indicate the dipolar origin of the generated incoherent second harmonic wave.

Introduction

The isolation of two-dimensional (2D) nanomaterials has attracted attention due to a myriad of applications in a diversity of areas, including optoelectronics and photonics[1-3]. In these areas, as well as in others, layered transition metal dichalcogenides (LTMDs) have stood out, with outstanding properties and performance[4,5]. Of particular importance to all-optical photonic devices, second-, third- and higher-order optical nonlinearities have been studied in 2D layered materials, and the nonlinear susceptibilities have been found to be higher than in their bulk (three-dimensional, 3D) counterparts, as reviewed in[6]. Although most of the work carried out so far exploit the semiconducting part of the 2D LTMDs' family, particularly MoX_2 and WX_2 (X = S, Se)[1-6], other 2D LTMDs have been isolated or synthesized by different methods, leading to metallic and semi-metallic nanomaterials. Within this group is Zirconium telluride, $ZrTe_2$, a group IVB LTMD[7], which has been prepared both in suspension and as a film on InAs (111) substrate[8]. Second-order nonlinearity has been well studied in the semiconducting LTMDs mentioned above, mainly through second harmonic generation [6,9]. However, in refs.[10, 11], hyper-Rayleigh scattering (HRS) was reported as means to characterize the second-order nonlinear susceptibility, $\boldsymbol{\chi^{(2)}}$, of liquid-exfoliated semiconducting tungsten disulfide, WS_2, monolayers. HRS is a technique first employed for studies of molecular solutions[12] and can be used to determine the orientation-averaged hyperpolarizability of molecules by correlating the intensity of the scattered second harmonic (SH) wave with the molecular concentration[13]. Recently, the technique was exploited to obtain the first-hyperpolarizability of subwavelength nanoparticles[14,15].

In the present work, we report on the first-hyperpolarizability measurement of colloidal dispersions of the semi-metallic $ZrTe_2$ 2D LTMD prepared via the redox exfoliation process[16,17]. This paper is organized as follows: we first summarize the monolayer $ZrTe_2$ preparation, following the method of refs.[16,17]. Then, we describe the HRS experiments and present the results, from which the orientation-averaged first-hyperpolarizability was found to be $\boldsymbol{\beta(2\omega) = (7.0 \pm 0.3) \times 10^{-24} esu}$ per $ZrTe_2$ monolayer flake, the largest reported so far for 2D LTMDs. By performing angular resolved intensity measurements, we confirmed the incoherent origin of the second harmonic emission. Polarization-resolved measurements were performed in the monolayer suspension and indicate a dipolar origin of the incoherent second harmonic generation.

[a]*Graduate Program in Materials Science, Universidade Federal de Pernambuco, Recife, PE 50670-901 Brazil*
[b]*Departamento de Física, Universidade Federal de Pernambuco, Recife, PE 50670-901 Brazil*
[c]*MackGraphe, Mackenzie Presbyterian University, São Paulo, SP 01302-907 Brazil. cjsdematos@gmail.com*
[d]*Materials and Manufacturing Directorate, Air Force Research Laboratories, 45433, Ohio, United States.*

Experimental Section

Synthesis and morphological characterization

The $ZrTe_2$ in 1T phase (space group $P\bar{3}m1$) nanoflakes were synthesized by a redox exfoliation method introduced by Jawaid and co-workers in 2017[16], whose detailed mechanism and application to other LTMDs materials have been recently described[17]. The $ZrTe_2$ flakes, with average lateral size of 118±53 nm and an average height of 1.54±0.91 nm, were obtained with measured heights expected to be higher than the actual flakes due to substrate-flake interactions. The synthesis details, as well as structural and morphological characterization including TEM (Transmission Electron Microscopy) images, AFM (Atomic Force Microscopy) profiles, XRD (X-Ray Diffraction) patterns and Raman spectroscopy are all detailed in the Supplementary Information.

Nonlinear Optical Experiment and Results

The experimental setup employed for the HRS measurements is shown in Figure 1. A Nd:YAG laser operating at 1064 nm, 10 Hz with pulses of 7 ns, was employed as the light source. A filter was used at the laser output to block any spurious radiation from the flashlamps. The input intensity on the sample was controlled by a combination of a half-wave plate and a polarizer.

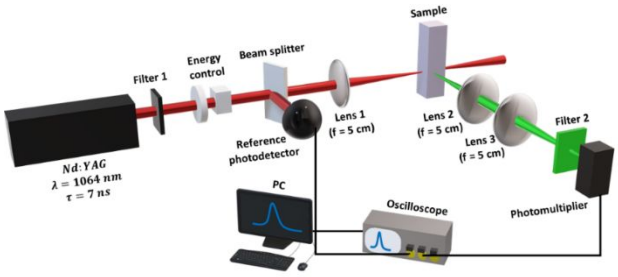

Figure 1 – HRS experimental setup (see text for details).

A beam splitter reflected part (10%) of the beam to a photodetector to monitor the input pulses. A 5 cm focal distance lens focused the beam on the sample, contained in a 10 mm x10 mm quartz cuvette. The scattered SH light was collected at an angle of 90° relative to the laser optical axis, using a pair of lenses with an interference filter (FWHM = 1 nm) after the lenses to allow only the SH of the 1064 nm laser beam to reach a photomultiplier (PMT). The forward beam was blocked by a beam-stopper. The data was acquired with a 300 MHz oscilloscope controlled by a computer. For spectral measurements, a PMT coupled to a monochromator was used. For these measurements, the layered $ZrTe_2$ nanoflakes were suspended in acetonitrile (ACN) at a concentration of 4.9 $x10^{10}$ particles/cm^3. To determine the first-hyperpolarizability, the external reference method was employed using para-nitroaniline (*p*-NA) as the reference standard[18].

Figure 2A shows the absorbance spectrum obtained with a UV-Vis-NIR, Cary 5000, Agilent Technologies. It can be seen that, for the $ZrTe_2$ nanoflakes concentration used in the experiments, the sample is virtually transparent in the visible and infrared ranges, with absorbances of 0.0019 and 0.0036 at 1064 nm and 532 nm (i.e., the laser's SH wavelength), respectively. No absorption peaks were observed in the visible and near infrared, indicating no electronic or excitonic transitions in this range, which is typical of metallic LTMDs. The increase in the absorbance towards the ultraviolet is attributed to electronic interband transitions in $ZrTe_2$.

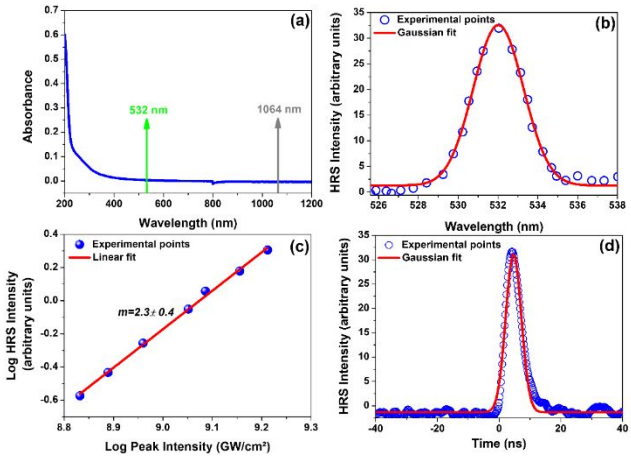

Figure 2 – (A) Absorbance spectrum for the ACN suspension of $ZrTe_2$; cell thickness: 10 mm. (B) HRS spectrum for the $ZrTe_2$ suspension. (C) Log - Log plot of the HRS output intensity versus the laser input intensity, showing the slope of the best linear fit. (D) Temporal profile of the HRS signal, following the input pulse duration (7ns). Concentration of nanoflakes: 4.9×10^{10} particles/cm^3.

Figures 2B and 2C show the spectral profile and the measured intensity dependence on laser intensity, respectively, obtained in the HRS experiment. Both the spectral peak at 532 nm and the quadratic intensity dependence are consistent with second harmonic generation. Figure 2D shows the temporal profile of the scattered signal, which resembles the laser profile, with a 7ns duration, that is also consistent with the fast response of the second-order nonlinear process, also indicating that the signal does not come from luminescence processes.
Measurements of the HRS signal intensity versus the volume concentration of the $ZrTe_2$ nanoflakes were performed and can be seen in Figure 3.

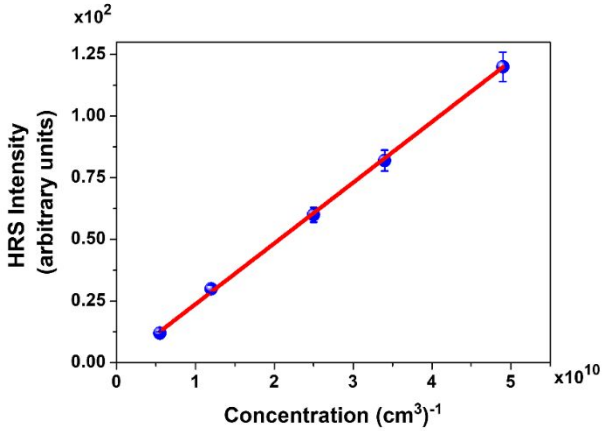

Figure 3 – HRS intensity as a function of $ZrTe_2$ nanoflakes

concentration. The linear behavior is indicative of no aggregation of the monolayers.

A linear behavior is observed for nanoflakes concentrations from $\mathbf{0.5 \times 10^{10} cm^{-3}}$ to $\mathbf{4.9 \times 10^{10} cm^{-3}}$, indicating that the SH signal is due to individual nanoflakes and not due to aggregates. No saturation was observed in the range of the laser intensities used.

To further confirm the incoherent nature of the second harmonic generation, we performed an angular measurement of the emitted SH intensity at the highest available peak intensity ~9.2GW/cm^2. The experimental setup for this measurement, shown in figure 4(a), was a modification of the original setup shown in fig.1. All the excitation path was kept as in fig. 1, but the collection part, with the same components, was mounted on a base which could be rotated from nearly 0^0 (almost parallel to the incident beam) to the forward direction (180^0). The obtained result is shown in figure 4(b) where, within the experimental error, a constant second harmonic signal is measured, without any evident enhancement therefore showing that there is no preferential direction for the SH emission. It confirms, therefore, that the SH signal is indeed incoherent in nature arising from HRS. For a literature comparison, in ref.[19] the authors studied angle resolved HRS in specific chromophores, where coherent contributions to the incoherent SH were detected by angular measurements showing an enhanced signal at a particular angle. When the signal was completely incoherent, as is the case here, the SH signal was constant as a function of angle.

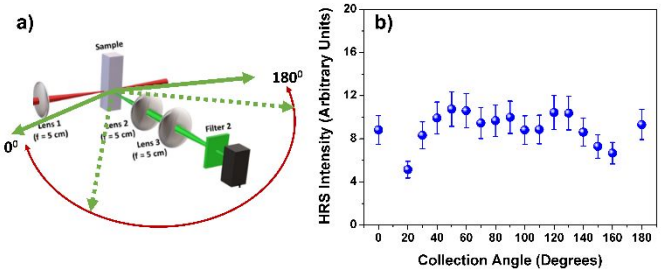

Fig. 4 – (a) Experimental setup for angular measurement of HRS signal; (b) Measured HRS SH signal intensity as a function of angle for a fixed input intensity of ~9.2GW/cm^2.

In order, to identify the origin of the SH light generated by the $ZrTe_2$ nanoflakes, polarization-resolved HRS experiments were performed. The experiments were carried out according to the usual procedure[20,21]. The incident laser beam was linearly polarized and the angle, $\boldsymbol{\gamma}$, between the optical field and the vertical direction was varied from 0 to $\boldsymbol{2\pi}$.

The intensity of the HRS signal along the direction perpendicular to the laser beam propagation was measured by placing an analyser in front of a photomultiplier and measuring the HRS intensity either in the vertical or horizontal (i.e., parallel to the incident beam propagation axis) direction. Figure 5 is a polar plot of the input polarization angle dependence of the HRS intensity. As discussed in the next section, the obtained profiles indicate an electric dipole origin for the SH generation[21]. The non-circular shape of the curve for the analyser in the horizontal orientation, Figure 5(b), is expected when the shapes of the particles are not centrosymmetric.

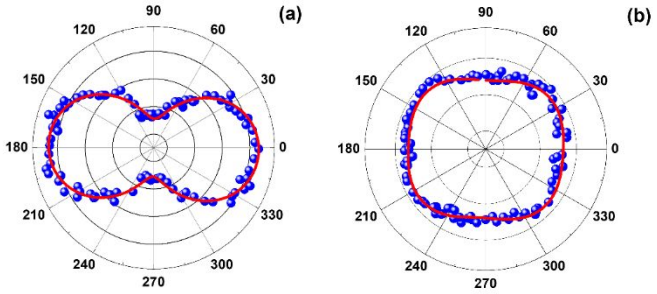

Figure 5. Polar plots of the HRS intensity generated by the nanoflakes in suspension versus the input laser polarization angle for detection along the direction perpendicular to the input beam propagation direction. Analyzer in the vertical (a) and horizontal (b) orientations.

Discussion

The theoretical treatment for the HRS data is well known[12,13], the employed external reference method is well established[20], and we highlight the main equations used to fit the data. The SH scattered light intensity by a composite sample can be described as[12]:

$$I(2\omega) = g\left\{\Sigma_c N_c F_c \langle \beta_c^2(2\omega)\rangle\right\} I^2(\omega), \qquad (1)$$

where $\boldsymbol{N_c}$ is the nonlinear particle concentration, $\boldsymbol{I(\omega)}$ is the incident laser intensity, $\boldsymbol{\beta_c(2\omega)}$ is the effective first-hyperpolarizability and the sub-index represents the constituents of the suspension. The brackets in the factor $\langle \boldsymbol{\beta_c^2(2\omega)}\rangle$ indicate orientational average and $\boldsymbol{F_c}$ is a local field factor given by $\boldsymbol{F_c = \{(n_{ACN}^2 + 2)/3\}}$[12, 22, 23], where $\boldsymbol{n_{ACN}}$ is the refractive index of ACN; the value calculated for this parameter is $\boldsymbol{F_c = 1.26}$. The factor g depends on the scattering geometry and contains information on the transformation of coordinates from the $ZrTe_2$ to the laboratory reference system[23, 24].

The HRS signal, $\boldsymbol{I(2\omega)}$, as a function of laser intensity for the two-component system studied can be written as

$$I(2\omega) = G\left(N_{sol}\langle\beta_{sol}^2\rangle + N_{solv}\langle\beta_{solv}^2\rangle\right) I^2(\omega), \qquad (2)$$

where *sol* stands for solute ($ZrTe_2$), $\boldsymbol{solv}$ stands for solvent (acetonitrile-ACN) in our case, and $\boldsymbol{G}$ is a parameter which includes local field correction and light collection efficiency.

For determination of $\langle \boldsymbol{\beta_c^2(2\omega)}\rangle$ we used the external reference method [12,24] according to

$$\langle\beta_{ZrTe_2}^2(2\omega)\rangle = \frac{I_{ZrTe_2}(2\omega)}{I_{p-NA}(2\omega)}\left\{\frac{N_{p-NA}\langle\beta_{p-NA}^2\rangle + N_{mOH}\langle\beta_{mOH}^2\rangle}{N_{ZrTe_2}}\right\} -$$

$$\frac{N_{ACN}\langle\beta^2_{ACN}\rangle}{N_{ZrTe_2}}, \quad (3)$$

where mOH refers to methanol, $\boldsymbol{\beta(2\omega)_{ACN} = 3.8 \times 10^{-31}\ esu}$ [25], $\boldsymbol{N_{ACN} = 1.3 \times 10^{22}}$ molecules/cm^3, $\boldsymbol{\beta(2\omega)_{p-NA} = 34 \times 10^{-30}\ esu}$[12], $\boldsymbol{N_{p-NA} = 1.0 \times 10^{19}}$ molecules/cm^3, $\boldsymbol{\beta(2\omega)_{mOH} = 0.69 \times 10^{-30}\ esu}$ [12], $\boldsymbol{N_{mOH} = 1.5 \times 10^{22}}$ molecules/cm^3. The volume concentration of $ZrTe_2$ monolayers was $\boldsymbol{N_{ZrTe_2} = 4.9 \times 10^{10}\ particles/cm^3}$, allowing for determining $\boldsymbol{\beta\ (2\omega) = (7.0 \pm 0.3) \times 10^{-24}\ esu}$. Notice that by using the "external reference method," knowledge of the parameter G is not necessary as can be seen in eq. (3).

The fitting of the polarization data shown in Figure 4 was performed using the following equation, which applies for emission of an electric dipole nature[20,21]:

$$I^{\Gamma}_{HRS} = a^{\Gamma}cos^4\gamma + b^{\Gamma}cos^2\gamma sin^2\gamma + c^{\Gamma}sin^4\gamma \quad (4)$$

where $\boldsymbol{I^{\Gamma}_{HRS}}$ is the HRS intensity and Γ corresponds to the H or V polarizations. The coefficients $\boldsymbol{a^{\Gamma}}$, $\boldsymbol{b^{\Gamma}}$and $\boldsymbol{c^{\Gamma}}$ were obtained by theoretical fit. The depolarization ratio $\boldsymbol{\rho^{\Gamma} = c^{\Gamma}/a^{\Gamma}}$ and the multipolarity, determined by $\boldsymbol{\zeta^{\Gamma} = 1 - (a^{\Gamma} + c^{\Gamma}/b^{\Gamma})}$, were calculated. From the experimental data, the values of these parameters, as well as of the coefficients in eq. (4) are given in Table I. The good fitting obtained, as well as the fact that $\boldsymbol{2a_H \approx 2c_H \approx b_H}$ and $\boldsymbol{c_H \approx c_V}$, are in line with a pure dipole nature for the SH radiation[20].

Table I – Coefficients of Eq. (4) determined from the polarization plots.

Coefficient	V polarization	H polarization
$\boldsymbol{a}$	0.89	0.33
$\boldsymbol{b}$	1.20	0.74
$\boldsymbol{c}$	0.27	0.25
$\boldsymbol{\rho}$	0.30	0.75
$\boldsymbol{\zeta}$	0.03	0.21

In order to compare the present results with the only previous report on HRS in TMDs[10, 11], we recall that the authors obtained $\boldsymbol{\beta(2\omega) = 2.66 \times 10^{-25}}$ *esu* for WS_2 nanoflakes, which are semiconductors, measured at the same optical wavelength (1064 nm) with 1 ns pulses. The $\boldsymbol{\beta(2\omega)}$ value herein reported for the semi-metal $ZrTe_2$ is larger by a factor 26.3 with respect to the WS_2 nanoflakes.

Note that $ZrTe_2$ in the 1T phase is centrosymmetric (from bulk all the way down to the monolayer)[26], meaning that the observed second-order nonlinearity is of a surface/edge nature, as with metallic nanoparticles[21]. The fact that the nonlinear scattering profile has a dipolar character indicates that it arises from the non-centrosymmetric shape of the nanoflakes[20] with important contributions from the nanoflakes edges. Also, the higher hyperpolarizability value obtained here relative to that obtained for the WS_2 in[10,11] is probably due to two further reasons: first, the number of $ZrTe_2$ atoms, because the nanoflakes have a higher average volume [Vol (WS_2) = 1500 nm^3 vs Vol ($ZrTe_2$) = 21443 nm^3]. Besides, as another reason, one should recall that the unit cell of $ZrTe_2$ has 144 electrons, which is more than the 106 electrons in the unit cell of WS_2. Thus, the nonlinear response of $ZrTe_2$ would be higher.

Conclusions

In conclusion, we reported on the first-hyperpolarizability of $ZrTe_2$ monolayers at 532 nm for excitation at 1064 nm. Hyper-Rayleigh Scattering experiments were performed with $ZrTe_2$ nanoflakes suspended in acetonitrile with concentrations varying from $\boldsymbol{0.5 \times 10^{10}\ cm^{-3}}$ to $\boldsymbol{.9 \times 10^{10}\ cm^{-3}}$. By measuring the HRS intensity dependence as a function of the laser intensity and using a solution of para-nitroaniline as a reference standard, a large first-hyperpolarizability of $\boldsymbol{(7.0 \pm 0.3) \times 10^{-24}\ esu}$ per monolayer flake was determined. The present results show that monolayer $ZrTe_2$ nanoflakes can act as efficient nonlinear electric dipoles.

Conflicts of interest

There are no conflicts to declare.

Acknowledgements

The authors thank the financial support from the Brazilian agencies: Conselho Nacional de Desenvolvimento Científico e Tecnológico (CNPq), Fundação de Amparo à Ciência e Tecnologia do Estado de Pernambuco (FACEPE), and Coordenação de Aperfeiçoamento de Pessoal de Nível Superior (CAPES). ASLG and CJSdM acknowledge support from AFOSR. AMJ, AJR, and RAV thank AFOSR and the Air Force Research Laboratory Materials and Manufacturing Directorate for financial support. CJSdeM acknowledges support from FAPESP (process nos. 2015/11779-4 and 2018/25339-4) and CAPES PrInt (process no. 88887.310281/2018-00).

References

1. P. Miró, M. Audiffred, and T. Heine *Chem. Soc. Rev.*, **2010**, 43, 6537.
2. S. A. Han, R. Bhatia, & S.-W. Kim, *Nano Convergence*, **2015**, 2. 17.
3. N. Huo, Y. Yang, & J. Li, J. Semicond., **2017**, 38, 031002 -1/9.
4. Z. Wei, B. Li, C. Xia, Y. Cui, J. He, J. –B. Xia, and J. Li, *Small Methods*, **2018,** 2, 1800094.

5. Z. Lin, A. McCreary, N. Briggs, S. Subramanian, K. Zhang, Y. Sun, et.al. *2D Mater.*, **2016**, 3, 042001.
6. A. Autere, H. Jussila, Y. Dai, Y. Wang, H. Lipsanen, and Z. Sun, *Adv. Mater.,* **2018**, 30, 1705963.
7. C. Yan, C. Gong, P. Wangyang, J. Chu, K. Hu, C. Li, et.al. Adv. Funct. Mater., **2018**, 1803305.
8. P. Tsipas, D. Tsoutsou, S. Fragkos, R. Sant, C. Alvarez, H. Okuno, et. al. *ACS Nano*, **2018**, 12, 1696–1703.
9. Y. Wang, J. Xiao, S. Yang, Y. Wang, and X. Zhang. *Opt. Mater. Express.* **2019***,* 9, 1136-1149.
10. T. G. Forcherio, J. Riporto, R. J. Dunklin, Y. Mugnier, R. Le Dantec, L. Bonacina, and D. K. Roper *Opt. Lett.* **2017**, 42, 5018-5021.
11. T. G. Forcherio, J. Riporto, R. J. Dunklin, Y. Mugnier, R. Le Dantec, L. Bonacina, and D. K. Roper *Opt. Lett.* **2017**, 43, 2400-2401.
12. K. Clays and A. Persoons *Phys. Rev. Lett*. **1991**, 66, 2980.
13. S. F. Hubbard, R. G. Petschek, and K. D. Singer, *Opt. Lett.* **1996***,* 21, 1774.
14. E. V. Rodriguez, C. B. de Araújo, A. M. Brito-Silva, V. I. Ivanenko, and A. A. Lipovskii, *Chem. Phys. Lett.,* **2009**, 467, 335–338.
15. R. Le Dantec, Y. Mugnier, G. Djanta, L. Bonacina, J. Extermann, L. Badie, et. al. *J. Phys. Chem. C*, **2011**, 115, 15140–15146.
16. A. Jawaid, J. Che, L. F. Drummy, J. Bultman, A. Waite, M.-S. Hsiao, and R. A. Vaia, *ACS Nano*, **11**, 2017, 635–646.
17. A. M. Jawaid, A. J. Ritter, and R. A. Vaia, Chem. Mater., 2020, 32, 6550–6565.
18. M. A. Pauley, H. -W. Guan, C. H. Wang, and A. K. -Y. Jen, ~~*The*~~ *J. Chem. Phys.***, 1996,** 104*,* 7821-7829.
19. K. Clays, K. Wostyn and A. Persoons, *Linear and Nonlinear Optics of Organic Materials, Manfred Eich, Mark G. Kuzyk, Editors, Proceedings of SPIE* **2001**, 4461, 105-116.
20. J. Nappa, G. Revillod, I. Russier-Antoine, E. Benichou, C. Jonin, & P. F. Brevet. *Phys. Rev. B,* **2005***,* **7***,* 165407.
21. J. Butet, A. Maurice, E. Bergmann, G. Bachelier, I. Russier-Antoine, C. Ray, O. Bonhomme, C. Jonin, E. Benichou, and P. F. Brevet., Multipolar second harmonic generation from metallic nanoparticles, in: *Metal Nanostructures for Photonics*, Edited by L. R. P. Kassab and C. B. de Araújo, Elsevier 2019.
22. E. Hendrickx, K. Clays, and A. Persoons, *Acc. Chem. Res.,* **1998,** 31, 675–683.
23. C. Joulaud, Y. Mugnier, G. Djanta, et al. *J Nanobiotechnol.* **2013**, 11, S8.
24. R. Barbosa-Silva, J. F. Silva, U. Rocha, C. Jacinto, and C. B. de Araújo, *J. Lumin.*, **2019**, 211, 121-126.
25. P. Kaatz, E. A Donley, and D. P. Shelton, *J. Chem. Phys.,* **1998**, 108*,* 849–856.
26. J. Ribeiro-Soares, R. M. Almeida, E. B. Barros, P. T. Araujo, M. S. Dresselhaus, L. G. Cançado and A. Jorio, *Phys. Rev. B*, **2014**, 90, 115438/1-10.